Asian Journal of Pharmaceutical Sciences 14 (2019) 40–51

Available online at www.sciencedirect.com

ScienceDirect

journal homepage: www.elsevier.com/locate/AJPS

Original Research Paper

Folate-targeted nanostructured chitosan/chondroitin sulfate complex carriers for enhanced delivery of bortezomib to colorectal cancer cells

Zar Chi Soe[a,b,1], *Bijay Kumar Poudel*[a,1], *Hanh Thuy Nguyen*[a,1], *Raj Kumar Thapa*[a], *Wenquan Ou*[a], *Milan Gautam*[a], *Kishwor Poudel*[a], *Sung Giu Jin*[c], *Jee-Heon Jeong*[a], *Sae Kwang Ku*[d], *Han-Gon Choi*[e], *Chul Soon Yong*[a,*], *Jong Oh Kim*[a,*]

[a] *College of Pharmacy, Yeungnam University, Gyeongsan 712749, Republic of Korea*
[b] *Department of Pharmaceutics, University of Pharmacy (Yangon), Yangon 11031, Myanmar*
[c] *Department of Pharmaceutical Engineering, Dankook University, Cheonan 31116, Republic of Korea*
[d] *College of Korean Medicine, Haany University, Gyeongsan 712715, Republic of Korea*
[e] *College of Pharmacy, Hanyang University, Ansan 426791, Republic of Korea*

ARTICLE INFO

Article history:
Received 14 August 2018
Revised 10 September 2018
Accepted 23 September 2018
Available online 20 October 2018

Keywords:
Bortezomib
Chitosan chondroitin sulfate
Colorectal cancer
Folic acid

ABSTRACT

Folate-targeting self-assembled nanoparticles (NPs) using biocompatible and biodegradable natural polymers chitosan (Cs) and chondroitin sulfate (Chs) were developed to address the major challenge in cancer treatment, the selective delivery of nanoparticles to the target site. In this study, we successfully incorporated a hydrophobic drug, bortezomib (Bor), into folic acid (FA)-conjugated Cs/Chs self-assembled NPs (Bor/Cs/Chs-FA) for colorectal cancer therapy. The particle size and polydispersity index of Bor/Cs/Chs-FA were ~196.5 ± 1.2 nm and ~0.21 ± 0.5, respectively. A pH-dependent release profile was observed, facilitating cancer cell-targeted drug release under an acidic tumor microenvironment. Moreover, *in vitro* data revealed enhanced cellular uptake and apoptosis in folate receptor-expressing colorectal cancer cells (HCT-116 and HT-29) as compared to that in lung cancer cells (A549), which do not express folate receptors. Furthermore, intravenous administration of Bor/Cs/Chs-FA in a HCT-116 bearing xenograft mouse model showed that the NPs were a safe and effective drug delivery system. The results suggest that folate-targeted nanoparticle can be effectively applied for efficient chemotherapy of colorectal cancer.

* Corresponding authors. College of Pharmacy, Yeungnam University, 214-1, Dae-Dong, Gyeongsan 712749, Republic of Korea. Tel: + 82 53 8102813.
E-mail addresses: csyong@yu.ac.kr (C.S. Yong), jongohkim@yu.ac.kr (J.O. Kim).
[1] ZC Soe, BK Poudel and HT Nguyen have contributed equally to this work.
Peer review under responsibility of Shenyang Pharmaceutical University.

https://doi.org/10.1016/j.ajps.2018.09.004

1. Introduction

Biodegradable natural polymer-based nanoparticles are highly accepted as drug delivery carriers for cancer treatment [1]. The third most common cancer, colorectal cancer is simultaneous occurrence of colon cancer and rectal cancer [2]. Chemotherapy is a common strategy for treatment of cancer; however, it has many undesirable side effects caused by chemotherapy interaction with healthy cells in the body [3,4]. Therefore, a new interdisciplinary field called nanomedicine has been developed to modify the fate of the drug in the body [5,6]. Overcoming mononuclear phagocyte system (MPS) can prolong the presence of drugs in systemic circulation; [7] this can be achieved by the presence of PEG on NPs surface [8]. The presence of targeting ligands on the surface of nanoparticles increases the intracellular delivery of drugs to specific targets [9]. Many surface receptors such as transferrin and folate receptors are expressed in several cancer cell types.

Folate receptors (FRs) are one of the most expressed receptors on cancer cells [10] although they are expressed in many cancer cell types, their expression levels are low in normal cells [11]. In particular, colorectal cancer cell lines, HT 29 and HCT116 have over expressed the folate receptor which can easily interact with folate targeted nanoparticles on their surface [12] and increases release and uptake of cargo drugs at colonic area. Therefore, folate-targeted PEG conjugated nanoparticles could potentially enhance the effect of chemotherapeutic agents by promoting intracellular concentration of entrapped chemotherapeutic agents [13]. Furthermore, FA-conjugated nanoparticles could enhance the residence time of entrapped drugs in the body by active and passive targeting tumor sites, which might reduce tumor cell resistance [14].

Chitosan nanoparticles are widely used for several biomedical applications as a drug delivery system [15]. The positively charged amino group of Cs, the polyanionic natural polymer, forms complexes with negatively charged polyelectrolytes to spontaneously result in nanoparticle formation [16]. Researchers have fabricated nanoparticles, tablets, pellets, microcapsules, beads, membranes, gels, and films by using Cs-based polyelectrolyte complexes (PECs) [17,18]. Chs, a natural polysaccharide, is an acidic mucopolysaccharide found in cartilage, bone, and connective tissue. It can form ionic complexes with positively charged chitosan [19]. Chs is mechanically and chemically stable and is an ideal matrix for many biomedical applications including site-specific drug delivery in chemotherapy and treatment of many diseases.

Recently, new drug delivery system was developed as PECs prepared from natural polysaccharides, including Cs and chondroitin sulfate (Chs) complexes [20] because interpolymer complexed nanocarriers for chemotherapy easily develop due to the attraction between (NH_3^+) of Cs and (-OSO_3^- and -COO^-) of Chs [21]. Moreover, this PECs have biological properties such as biocompatibility, biodegradability and produce better carriers for ionized drugs with high drug loading and entrapment efficiency [22].

Bortezomib (Bor), used in the treatment of multiple myeloma, is an inhibitor of the 26S proteasome [23]. It is also used as chemotherapeutic drug in many cancers such as hepatocellular carcinoma, prostate cancer, ovarian cancer, and colon cancer [24]; it also inhibits transcription factor nuclear factor-kappa beta (NF-kB). Bor increases the cellular susceptibility of cancers to apoptosis by inhibiting NF-kB [25].

In the present study, we developed a Bor-loaded natural polysaccharide nanoparticle system conjugated with folate-coupled DSPE-PEG (Fig. 1). PEG moiety in the amphiphilic DSPE-PEG could promote and prolong the blood circulation, whereas the DSPE moiety could increase the drug loading capacity and stability of the core. FA will act as a targeting ligand to increase the uptake of drug in colorectal cancer cell lines. We studied the therapeutic activity of Bor/Cs/Chs-FA nanoparticles *in vitro* and in tumor bearing xenografts mice model as *in vivo*.

2. Materials and methods

2.1. Materials

Bor was obtained from LC Laboratories (Woburn, MA, USA). Cs, Chs, FA, and MTT [2,5-diphenyltetrazolium bromide] were purchased from Sigma-Aldrich (St Louis, MO, USA). HCT-116, HT-29, and A549 cells were obtained from the Korean Cell Line Bank (Seoul, South Korea). DSPE-PEG_{2000} was purchased from Avanti Polar Lipid (Alabaster, AL, USA). Coumarin-6 and Lyso Tracker Red were purchased from Thermo Fisher Scientific Inc. (Waltham, MA, USA). Primary antibodies, ubiquitin, and P53 were purchased from Cell Signaling Technology (Danvers, MA, USA). All other chemicals were of reagent grade and used without further purification.

2.2. Preparation of cs/chs NPs and Bor/Cs/Chs-FA

Cs/Chs, Bor/Cs/Chs, and Bor/Cs/Chs-FA NPs were prepared by polyelectrolyte complexation between carboxylate and sulfate groups from chondroitin sulfate and amino groups of chitosan [26]. Briefly, stock solutions of Cs (1.5 mg/ml, pH = 4.5) and Chs (1.75 mg/ml, pH = 6.5) were prepared using purified water. The stock solutions were filtered using 0.2 μm filter paper (Whatman, Dassel, Germany) and diluted to optimized concentrations. Cs/Chs NPs were prepared by mixing Cs and Chs with stirring at 25 °C. Different concentrations of Chs (0.41–1.25 mg/ml) were added into 1.5 mg/ml Cs solution to get desired Chs/Cs weight ratios (1:6). For preparation of Bor/Cs/Chs and Bor/Cs/Chs-FA, firstly, Bor and FA-conjugated DSPE-PEG, which was prepared and characterized in a previous study [27], were dissolved in phosphate buffer saline. Bor solution was then added to the Chs solution dropwise with stirring at room temperature and kept for 6 h. Finally, FA-conjugated DSPE-PEG was added to the Bor-loaded Cs/Chs NPs, (Bor/ Cs&Chs weight ratios, 1:2) with stirring and kept for 12 h at 25 °C. The resulting solution was centrifuged at 13 000 rpm for 25 min at 20 °C and the NP pellet was re-suspended in purified distilled water after discarding the supernatant to obtain Bor/Cs/Chs-FA (Bor/ Cs&Chs/FA weight ratios, 1:2:1) for further study of *in vitro* and *in vivo* experiments.

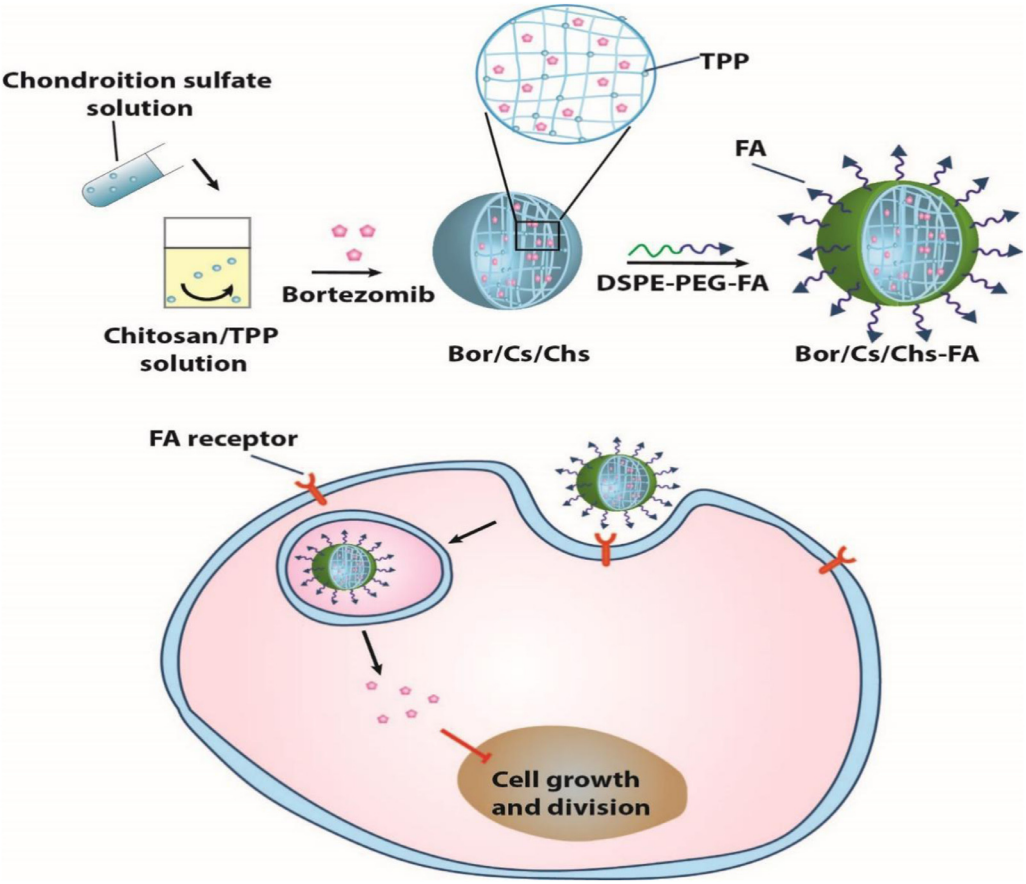

Fig. 1 – Schematic illustration of preparing folate targeted polymeric nanoparticles to deliver bortezomib to folate receptor expressing colorectal cancers.

2.3. *Morphological analysis of cs/chs NPs and Bor/Cs/Chs-FA*

The morphology of Cs/Chs NPs and Bor/Cs/Chs-FA was studied using Transmission Electron Microscope (CM 200 UT, Philips, MA, USA). Briefly, samples stained with phosphotungstic acid solution were put on copper grid, which was coated with carbon and dried at room temperature. Transmission electron microscope was operated at 120 kV to take images of NPs [28].

The physicochemical properties of nanoparticles such as zeta-potential, polydispersity index (PDI), and Z-average hydrodynamic particle size were characterized using the DLS (dynamic light scattering) method with a Zetasizer Nano ZS (Malvern Instruments, Malvern, UK) [29,30] on Nano DTS software (version 6.34). Three individual measurements were taken to obtain mean value.

FTIR spectra of dried Bor/Cs/Chs and Bor/Cs/Chs-FA were obtained using an FTIR spectrophotometer (Thermo Scientific Nicolet Nexus 670) and compared with Bor, Cs, and Chs spectra [31].

2.4. *Drug loading and encapsulation efficiency*

To estimate the entrapment efficiency (EE) and loading capacity (LC) of Bor in Bor/Cs/Chs-FA, we used an Amicon® centrifugal filter device (molecular weight cut-off, 10 000 Da, Millipore) [32]. Unbound drug in Bor/Cs/Chs-FA was separated by centrifugation for 10 min at 5000 rpm; filtrate was analyzed on an HPLC system (Hitachi, Japan), which comprised: an L-2130 pump, L-2200 autosampler, L-2420 UV–Vis detector, L-2350 column oven, and Ezchrom elite software (318a, Japan) [33]. PBS (pH 7.4): methanol (50:50, v/v) was used as a mobile phase for isocratic elution and an Inertsil C_{18} column (150 mm × 4.6 mm, 5 µm particle size, Cosmosil, Nacalai Tesque Inc., USA) was used as the stationary phase. A 20 µl sample was injected; the flow rate of the mobile phase was 1.0 ml/min and column temperature was 25 °C. UV absorbance was detected at a wavelength of 278 nm. The percentages of EE and LC were calculated according to the following equations:

$$\text{EE (\%)} = \frac{W_D}{W_T} \times 100$$

where W_D is the weight of Bor encapsulated in Bor/Cs/Chs-FA and W_T is the total weight of Bor when preparing the formulation.

$$\text{LC(\%)} = \frac{W_D}{W_{TN}} \times 100\%$$

where W_D is the weight of Bor encapsulated in Bor/Cs/Chs-FA and W_{TN} is the total weight of nanoparticles including the amount of adding Bor, and total weight of Cs/Chs.

2.5. *In vitro drug release study*

In vitro release rate of Bor from Bor/Cs/Chs and Bor/Cs/Chs-FA was studied in phosphate-buffered saline (PBS; physiological pH 7.4) and acetate-buffered saline (ABS; acidic pH 5.0) using a dialysis membrane (Spectra/Por 3500 Da-MWCO) [34]. Predetermined volume of formulation was added to the dialysis membrane and it was immersed in 30 ml of either ABS (0.01 M, pH 5.0) or PBS (0.01 M, pH 7.4). Release study was carried out at 37 °C with shaking at 100 rpm. At specified time points, samples were collected and aliquots of fresh media were replaced. The amount of Bor release was calculated by HPLC method as described in Section 2.3.

2.6. *Stability of Bor/Cs/Chs and Bor/Cs/Chs-FA*

The most important parameter to characterize the optimization of formulated nanoparticles is the stability of created drug loaded nanoparticles [35]. For physical stability, Bor/Cs/Chs and Bor/Cs/Chs-FA were kept at 4 °C and room temperature, 40 °C and the content of drug and particle size were determined at specified time point. The stability of Bor/Cs/Chs and Bor/Cs/Chs-FA in physiological condition was carried out in plasma obtained from the blood of mice by loading Bor/Cs/Chs and Bor/Cs/Chs-FA in plasma and the mixture of formulations and plasma was kept in shaking incubator at 40 °C. The amount of drug content in nanoparticles and particle sizes were measured at predetermined interval [36].

2.7. *Cellular cytotoxicity of Bor/Cs/Chs-FA*

The cytotoxic effect of Bor/Cs/Chs-FA was determined by using MTT assay (Promega, USA) [37]. The percentage cell viability after treatment with Bor/Cs/Chs-FA was compared with those of free Bor and Bor/Cs/Chs in HT-29 and HCT-116 cells (folate receptor expressing cancer cell lines) and A549, lung cancer cells (cell line that does not express folate receptors). All cells (1×10^4/well) seeded in 96-wells plates were incubated for 24 h and treated with Cs/Chs NPs, Bor, Bor/Cs/Chs, Bor/Cs/Chs and Bor/Cs/Chs-FA. After treatment with MTT, absorbance was determined at 570 nm by using an automated microplate reader. Untreated cells were designated as controls and the percentage cell viability of each cell line was calculated using the following formula.

$$\text{Cell viability}(\%) = \frac{\text{A570(sample)} - \text{A570(blank)}}{\text{A570 (control)} - \text{A570(blank)}} \times 100$$

Where, A is the absorbance.

2.8. *Cellular uptake efficacy of Bor/Cs/Chs-FA*

To study the localization and uptake of drug carrier in both folate receptor expressing and deficient cell lines, confocal laser scanning microscopy was used. All cells (1×10^5/ well) were seeded in 12-wells plates containing cover slips. After 24 h, coumarin-6-loaded folate targeted nanoparticles were added to each well, followed by staining with Lyso Tracker® Red (1 µl) for 10 min. Cells in one group from each cell line were treated with FA (20 µg) for one hour as pretreatment to quantify the uptake of folate-targeted nanoparticles via folate receptors. All treated cells were kept in the dark and fixed with 4% paraformaldehyde solution. For visualization under confocal laser scanning microscope (Leica Microsystems, Wetzlar, Germany), the cover slips containing treated cells were mounted on glass slides and sealed with glycerin [38].

The uptake of folate-targeted nanoparticles was studied using fluorescence-activated cell sorting (FACS; BD Biosciences, San Jose, CA, USA). Folate receptor expressing cell lines, HCT-116 and HT-29 (1×10^5/ well), were seeded in 12 wells plates and incubated for 24 h. Subsequently, different concentrations of coumarin-6-loaded targeted nanoparticles were added to the cells at predetermined times. The same procedure was performed for folate receptor deficient A549 cell line. To confirm the folate receptor-mediated uptake efficacy of formulations, one group of cells was pretreated with free FA (20 µg). Finally, cells were collected, washed and dispersed in 0.5 ml PBS, and analyzed [32].

2.9. *In vitro cellular study*

To investigate cell cycle status including cell replication, proliferation, and division at four critical stages (G1, S, G2, and M), cell cycle analysis was carried out using a fluorescence assay kit (Cell Clock ™; Biocolor Ltd., UK). Briefly, after incubation for 24 h, cells (1×10^5/ well in a 12-wells plate) were treated with Bor, Bor/Cs/Chs, and Bor/Cs/Chs-FA, and then incubated for another 24 h. Cells were then stained with a redox dye (Cell-Clock Dye Reagent) for 1 h at 37 °C and imaged using a fluorescence microscope (Nikon Eclipse Ti). The number of cells arrested in each phase from digitized photomicrographs was determined using ImageJ software [39].

To determine the toxicity of Bor/Chs/Cs-FA against both folate receptor expressing and deficient cell lines, live/dead assay was performed [40]. Briefly, cells (1×10^5 /well) were seeded in a 12-well plate, and treated with Bor, Bor/Cs/Chs, and Bor/Cs/Chs-FA followed by incubation for 24 h. Subsequently, cells were washed with PBS and then stained with propidium iodide (red fluorescence) and acridine orange (green fluorescence). Finally, the cells were observed under a fluorescence microscope (Nikon Eclipse Ti, Nikon Instruments Inc.).

A cell migration study was performed to estimate the anti-metastatic effect of Bor/Cs/Chs-FA. Cells (1×10^5 /well in 12-well plates) were seeded and incubated for 24 h. To get a straight cell-free 'scratch', the monolayer of cells was scraped off using a pipette tip. The cells from the scraped area were removed by washing with PBS and images were taken (designated as 0 h). Then, cells were incubated for 24 h with Bor, Bor/Cs/Chs, and Bor/Cs/Chs-FA. Subsequently, the cells were photographed and the images were compared with those taken at 0 h [41].

2.10. *Western blot analysis*

All cells (2×10^5 /well) were seeded in 6-wells plates. After 24 h, all seeded cells were incubated with Bor, Bor/Cs/Chs, and Bor/Cs/Chs-FA for another 24 h. Then, the cells were harvested, lysed, and incubated for 40 min on ice with proteinase inhibitors. The reaction mixture was then centrifuged at 13 000 rpm for 20 min at 4 °C, and the supernatant obtained was

used to quantify the concentration of proteins using a BSA Protein Assay Kit (Thermo Scientific, IL, USA). Bis-Tris polyacrylamide gel (10%) was used to separate proteins, which were then transferred to polyvinylidene fluoride membrane. After blocking with 5% nonfat milk powder suspension, the membranes were incubated overnight with primary antibodies, GAPDH, p53, and Ubiquitin. The expression levels of proteins were determined after incubation with suitable secondary antibodies for 1 h using enhanced chemiluminescence [33].

2.11. *In vivo antitumor effects*

A tumor xenograft model was developed by injecting HCT-116 cells (1×10^7) into the right flanks of female balb/c nude mice to examine *in vivo* antitumor efficacy of Bor, and its formulations with and without folate targeting. The experimental animals were randomly grouped into control and three other experimental groups (Group 1: control, Group 2: Bor, Group 3: Bor/Cs/Chs and Group 4: Bor/Cs/Chs-FA). When the tumor volumes reached approximately 100 mm^3, free drug and different formulations were injected three times every four days via the tail vein. The length and width of tumors were measured by using Vernier calipers and volume was calculated as:

$$V = \frac{(Width)^2 \times Length}{2}$$

Moreover, loss of body weight, which is one of the parameters used to characterize the toxicity of Bor/Cs/Chs-FA, was also determined. At the end of the study, all mice were sacrificed by CO_2 inhalation to harvest tumors and principal organs following the protocols of the Institutional Animal Ethical Committee of Yeungnam University, South Korea. All tumors and organs were fixed in formalin for immunohistochemical assay. The experiments were approved by the Institutional Animal Ethical Committee, Yeungnam University, South Korea [33].

2.11.1. *Histopathological characterization*

The specimens extracted from mice bearing HCT-116 tumors were cut (3–4 μm) and studied using an optical microscope (Nikon Corporation, Tokyo, Japan) after staining with hematoxylin and eosin (H&E). Furthermore, computer-based automated image analyzer (iSolution FL ver 9.1; IMT i-solution Inc.; Vancouver, Quebec, Canada) was used to estimate tumor cell volumes from intact tumor cell-occupied regions (% mm^{-2} of tumor mass) [42,43].

2.11.2. *Immunohistochemistry*

The levels of CD31, Ki-67, caspase-3, and PARP in extracted tumors were determined using a combination of specific antibodies, an avidin–biotin–peroxidase complex (ABC), and a peroxidase substrate kit (Vector Labs, Burlingame, CA, USA). Briefly, tissue sections were incubated with methanol and 0.3% H_2O_2 and then blocked by incubation with nonspecific immunoglobulins and endogenous peroxidase. Samples were then incubated for 1 h in a humidified chamber at 95–100 °C, washed with 10 mM citrate buffer (pH 6.0), and blocked using normal horse serum. Subsequently, the samples were treated with primary antisera and incubated at 4 °C overnight. All samples were incubated for 1 h at room temperature with biotinylated universal secondary antibodies and ABC reagents and rinsed 3 times with PBS between each step. The samples were noted as positive for apoptosis if the sections were covered by 20% or more of each marker (caspase-3 and PARP) for apoptosis. An automated image analyzer was used to calculate the area (% mm^{-2} of tumor mass) occupied by caspase-3 and PARP-positive cells located in the tumor mass [44,45].

2.11.3. *In vivo imaging and biodistribution analysis*

Qualitative and quantitative distribution of Cy 5.5-loaded targeted nanoparticles and Cy 5.5-loaded non-targeted nanoparticles were studied in mice bearing HCT-116 tumors after tail vein injections (100 μl of samples containing 1 μg/ml Cy 5.5). The fluorescence intensity of Cy 5.5 was determined at 1, 6, 12, and 24 h using FOBI fluorescence imaging system (Neoscience Co.Ltd). After 24 h, the fluorescence intensity in healthy organs (spleen, heart, lung, liver, and kidneys) and tumors was also estimated [46].

2.12. *Statistical analysis*

To determine the statistically significant differences between the groups in all experiments, Student's *t*-test (for pairs of groups) and one-way analysis of variance (ANOVA) were used. All data are presented as the mean ± standard deviation (SD) and $P < 0.05$ was considered statistically significant.

3. Results and discussion

3.1. *Preparation and characterization of Bor/Cs/Chs-FA*

In this study, we developed Bor-loaded polymeric nanoparticles by using different ratios of natural polymers (chitosan and chondroitin sulfate) with folate targeting DSPE-PEG. The optimized nanoparticles had Chs: Cs at a ratio of 1:6, and a particle size of 165.2 ± 0.9 nm. After drug loading, the nanoparticle size was 174.7 ± 0.7 nm; Bor/Cs/Chs-FA was larger with a size of 186.5 ± 1.2 nm. All nanoparticles had a narrow size distribution as shown by polydispersity index (PDI) values (Fig. 2A). In addition, excess of the amine groups of chitosan as compared to the sulfate group of chondroitin sulfate resulted in the overall positive charge, as shown by zeta potential (Fig. 2B).

The morphology of Cs/Chs NPs, Bor/Cs/Chs, and Bor/Cs/Chs-FA was characterized by TEM (Fig. 2C). Results showed that the nanoparticles were successfully coated by folate-targeted DSPE-PEG. Moreover, the nanoparticles had small particle sizes (~200 nm) and were distinct and discrete spherical particles [40].

To determine the effects of drug loaded in Bor/Cs/Chs-FA, drug loading capacity and encapsulation efficiency are very important parameters. Bor/Cs/Chs-FA was prepared with different ratios of Chs and Cs to study the encapsulation efficacy of drugs [47]. In this study, we selected Chs/Cs ratio of 1:6 for preparation of nanoparticle because it has high Bor loading capacity (98.5%) and encapsulation efficiency (21.4%) (Fig. 2D). In addition, to characterize the chemical interaction of drugs with folate targeting or polymeric components, FTIR analysis

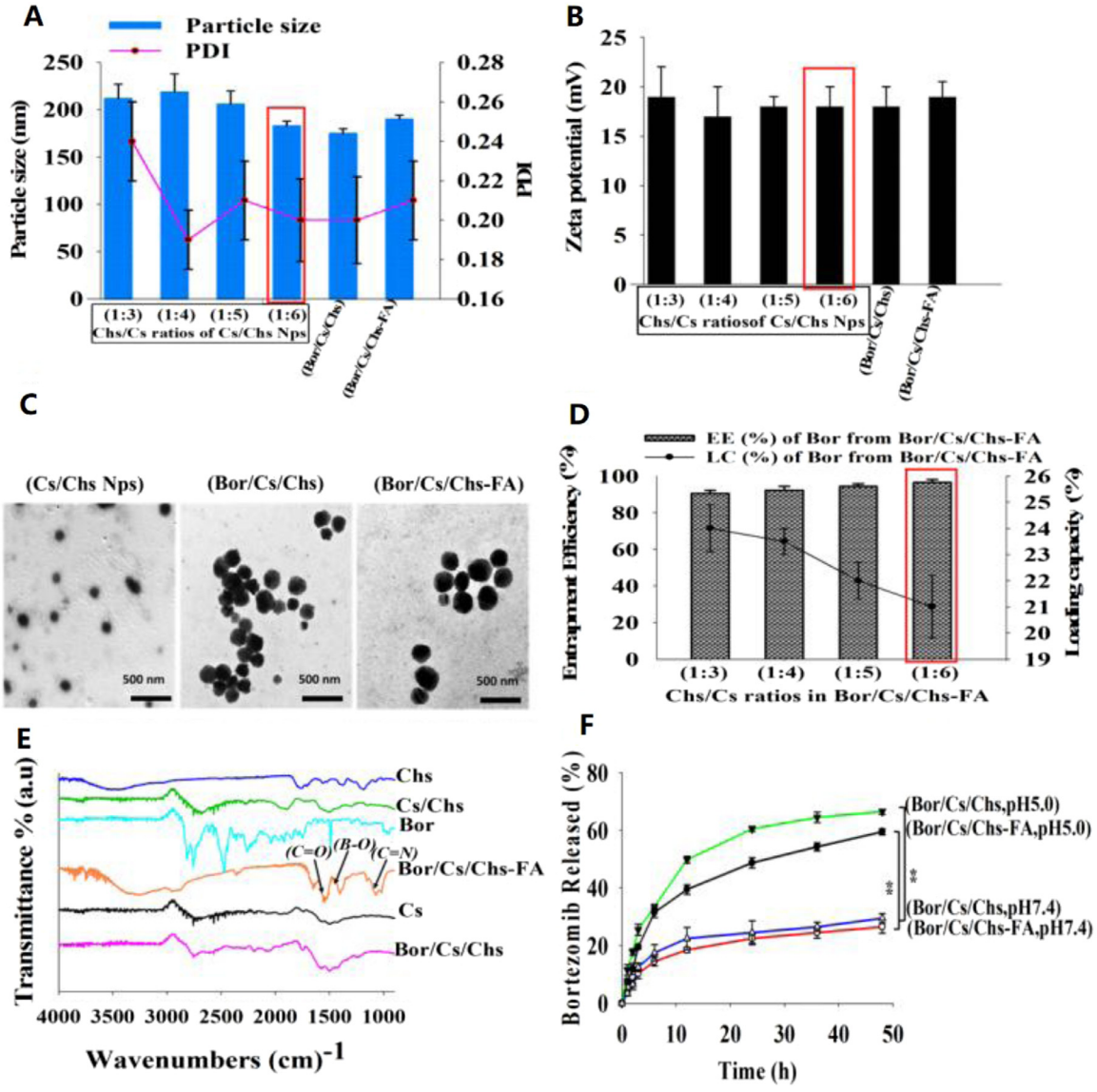

Fig. 2 – Physicochemical characterization of Bor/Cs/Chs-FA (Bor/Cs&Chs/FA weight ratios, 1:2:1). (A) Particle size and PDI, (B) Zeta potential of blank polymeric nanoparticle with different ratios of Chs and Cs, Bor/Cs/Chs, and Bor/Cs/Chs-FA. (C) TEM images of Bor/Cs/Chs and Bor/Cs/Chs/-FA. (D) Percentage entrapment efficiency and loading capacity of bortezomib in Bor/Cs/Chs-FA with different ratios of Chs and Cs. (E) FTIR spectra of Bor, Cs, Chs, and formulation with folate targeting ligand and without folate targeting ligand. (F) *In vitro* release profiles of Bor from Bor/Cs/Chs and Bor/Cs/Chs-FA at pH 5.0 and pH 7.4. Data are shown as mean ± SD (n = 6) (*P < 0.05, **P < 0.01, ***P < 0.001).

was performed (Fig. 2E). The spectra of Bor/Cs/Chs-FA showed characteristic peak at 1275 cm^{-1} (C = N stretch), 1401 cm^{-1} (strong B-O stretching of bortezomib), and 1720 cm^{-1} (C = O, PEG layer). Bor was thus successfully loaded in Bor/Cs/Chs-FA.

The release rate of Bor from Bor/Cs/Chs and Bor/Cs/Chs-FA was evaluated at pH 7.4 (PBS) and pH 5.0 (ABS) using dialysis membrane (Fig. 2F). The release of Bor from both Bor/Cs/Chs and Bor/Cs/Chs-FA showed significant increase at acidic pH as compared with physiological pH. Moreover, the release rate from Bor/Cs/Chs-FA was slightly slower than that from Bor/Cs/Chs. This may be due to rapid distribution and enzymatic degradation of free drug from Bor/Cs/Chs in systemic circulation; moreover, delivery of drugs loaded in targeted nanoparticles results in controlled release at tumor site. Furthermore, chitosan is easily dissolved in acidic media, resulting in the release of drug and conjugate layer in acidic environment of tumor site, leading to increased antitumor efficacy and reduced untoward effects to healthy tissue [48].

Stability of Bor/Cs/Chs and Bor/Cs/Chs-FA was examined in physiological state, plasma media and at two different storage temperatures (4 °C and 40 °C) by measuring particle sizes, PDI, zeta potential and amount of drug contents in nanoparticles [49]. According to the results of hydrodynamic diameter, PDI and zeta potential of Bor/Cs/Chs and Bor/Cs/Chs-FA at two different temperatures (Fig. S1), created nanoparticles, both targeted and non-targeted nanoparticles have efficient stabil-

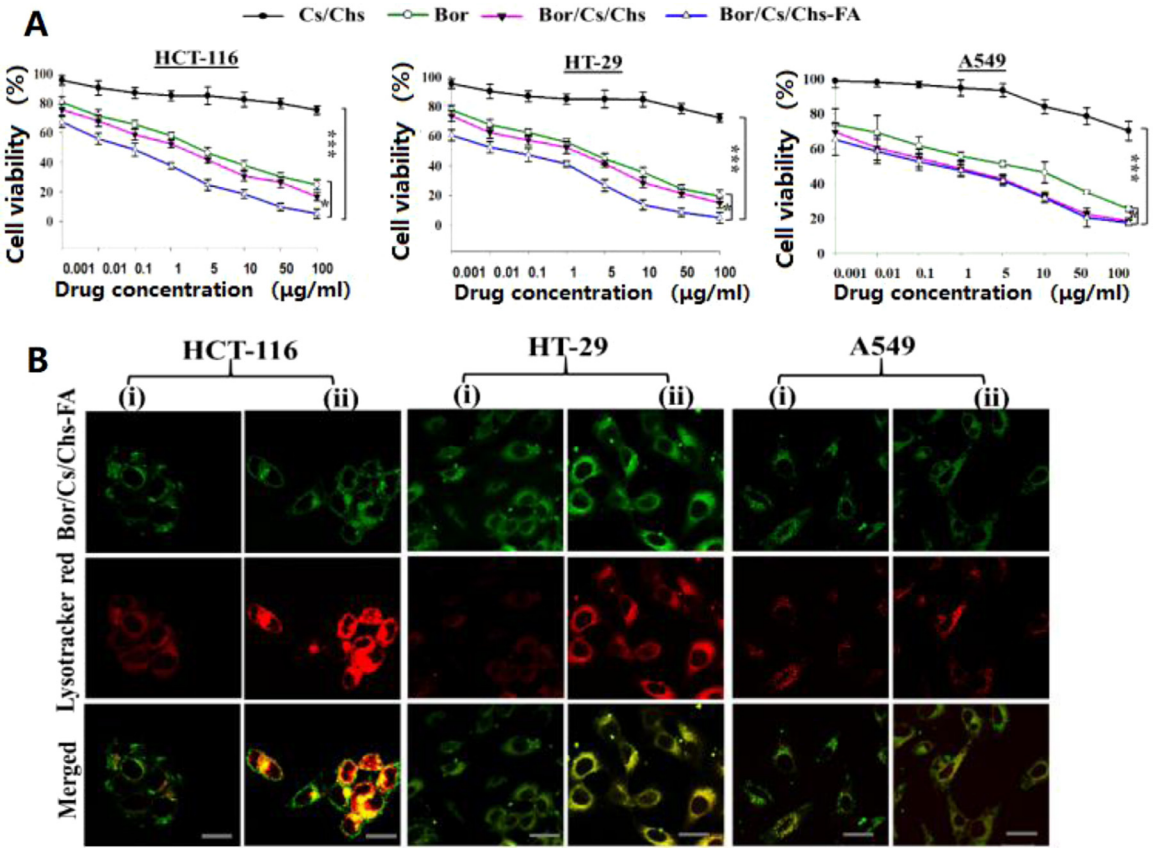

Fig. 3 – (A) *In vitro* cytotoxicity effect of Bor, Cs/Chs NPs, Bor/Cs/Chs, and Bor/Cs/Chs-FA (Bor/Cs&Chs/FA weight ratios, 1:2:1) at different concentration on folate receptor positive colorectal cancer cells, HCT-116 and HT-29, and folate receptor negative lung cancer cell line, A549. Data are shown as mean ± SD (n = 6) (*P < 0.05, **P < 0.01, ***P < 0.001). (B) Confocal images for cellular uptake of Coumarin-6-loaded targeted nanoparticles with lysotracker red in HCT-116, HT-29, and A549 cells (i) with pretreatment of FA, (ii) without pretreatment of FA. Scale bars represent 100 μm (For interpretation of the references to color in this figure legend, the reader is referred to the web version of this article.).

ity at different temperatures because there was no significant difference in measurement of hydrodynamic diameter, PDI and zeta potential. The electrostatic attraction between Cs and Chs was successfully developed to form polyelectrolyte complex. Similarly, the optimized stability of Bor/Cs/Chs-FA in physiological condition had been proved by estimating the contents of drug in nanoparticles and hydrodynamic diameter, PDI and zeta potential of Bor/Cs/Chs and Bor/Cs/Chs-FA after loading with plasma. The results were shown in (Fig. S2). Entrapment efficiency of Bor in Bor/Cs/Chs-FA was more than that of Bor/Cs/Chs and it was supported that DSPE-PEG in folate targeted ligand used in created formulation protected the drug from unwanted release before reaching the targeted area and RES clearance.

3.2. *Cytotoxicity of Bor/Cs/Chs-FA*

The cytotoxicity of Bor/Cs/Chs-FA was evaluated in both folate receptor expressing colorectal cancer cell lines (HCT-116 and HT-29) and folate receptor deficient lung cancer cell line (A549) [30] (Fig. 3A). Cs/Chs NPs showed cytotoxic effect on all three cell lines at concentrations >50 μg/ml. These results are in line with those of some previous studies, which reported that chitosan has significant biological activities, including immuno-enhancing effects, antimicrobial activities, wound healing, and antitumor activities [50]. As expected, Bor/Cs/Chs-FA was more cytotoxic in folate receptor positive cell lines (HCT-116 and HT-29) than free drug and Bor/Cs/Chs were. In contrast, the cytotoxicity of Bor/Cs/Chs-FA in A549 cell line was similar to that of non-targeted nanoparticles Bor/Cs/Chs, because A549 cell line lacks folate receptors. IC_{50} values of Bor and Bor/Cs/Chs-FA confirmed these results. To determine the IC_{50} values, standard curves were plotted by using the cytotoxicity profiles (Fig. S3). IC_{50} values of Bor/Cs/Chs-FA in both folate receptor expressing colorectal cancer cell lines were lower than in folate receptor deficient lung cancer cells (Table S1).

3.3. *Intracellular uptake and targeting potency of Bor/Cs/Chs-FA*

In this study, colocalization of coumarin-6-loaded folate targeted nanoparticles in all cells were observed using confocal microscopy. Most coumarin-6-loaded folate targeted nanoparticles (green) were localized around the perinuclear region of both folate receptor-expressing cell lines, suggest-

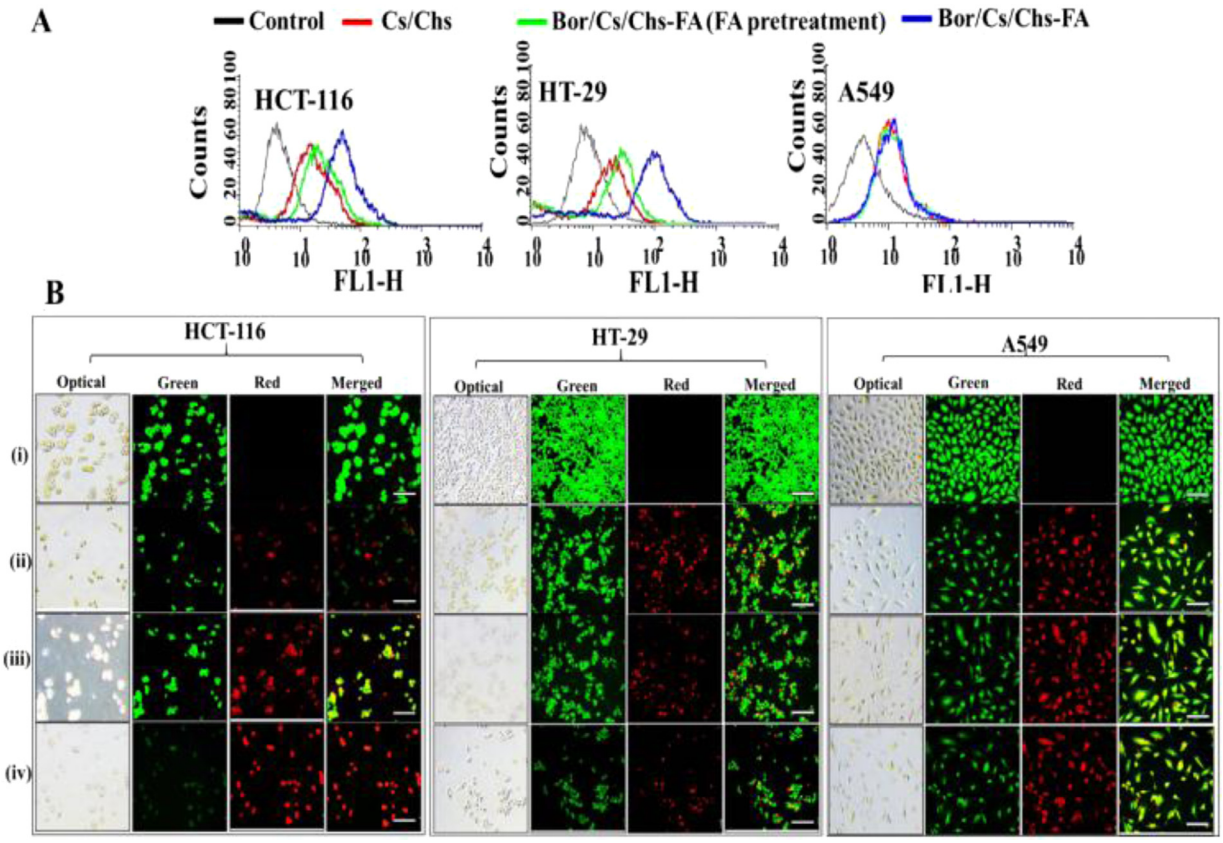

Fig. 4 – (A) Quantitative cellular uptake of coumarin-6-loaded targeted nanoparticles in different cell lines determined by using FACS; cells were either pretreated with FA or were without FA pretreatment. (B) Fluorescence microscopic images of folate receptor positive human colorectal cancer cells, HCT-116 and HT-29, and folate receptor negative lung cancer cell line, A549, incubated with (i) control, (ii) Bor, (iii) Bor/Cs/Chs, and (iv) Bor/Cs/Chs-FA (Bor/Cs&Chs/FA weight ratios, 1:2:1) for 24 h were taken after staining with Live/Dead assay kit contents; green or red fluorescence is defined as live or dead cells, respectively. Scale bars represent 100 μm (For interpretation of the references to color in this figure legend, the reader is referred to the web version of this article.).

ing that these nanoparticles were distributed into the cytoplasm. There was minimum uptake in FA pretreatment group. Moreover, the uptake of FA-targeted nanoparticles in these cell lines was markedly inhibited by the presence of excess amounts of free folic acid. It suggested that the uptake of targeted nanoparticles depended on the folate receptor mediated endocytosis. Furthermore, the role of folate ligand in cellular uptake mechanism was confirmed in A549 cells, which showed no significant change of uptake with or without FA pretreatment (Fig. 3B) [38].

Moreover, qualitative time- and concentration-dependent uptake profile of coumarin-6-loaded folate-targeted nanoparticles was examined in both folate receptor expressing and deficient cell lines by using FACS analysis (Fig. S4). The fluorescence intensity was increased when the dose (1–5 μg) and treatment time (30–90 min) were increased. However, there was no significant change in fluorescence intensity in A549 cell line, although treatment time and concentration were increased. Furthermore, the role of folate ligand in cellular uptake of targeted nanoparticles was confirmed by low uptake in folic acid pretreatment group of folate receptor expressing HCT-116 and HT-29 cells (Fig. 4A) [51].

Furthermore, quantitative cell death was examined in all cells treated with free drug and formulations with and without folate targeting ligand by sequential treatment with acridine orange (AO) and propidium iodide (PI) to distinguish the live and dead cells [52]. All cells treated with free drug showed more dead cells as compared to in the control group. HCT-116 and HT-29 cells treated with Bor/Cs/Chs-FA had higher cell death rate than A549 cells had (Fig. 4B). This could be attributed to the higher nanoparticle internalization in folate receptor overexpressing colorectal cancer cells as compared to folate receptor deficient cells.

Cell cycle analysis was performed to study the cell division and proliferation of all three cell lines following treatment with Bor, Bor/Cs/Chs, and Bor/Cs/Chs-FA using a redox dye, which changes color according to the cell cycle phases (G1, S, G2, and M) [39]. Bor/Cs/Chs-FA treated group in HCT-116 and HT-29 cell lines only had cell population with G1 phase, whereas cell population was observed in all phases in A549 cells. However, Bor and Bor/Cs/Chs treated groups showed cells in M and S phase (Fig. 5A, S5). This shows that cell cycle arrest after treatment with Bor/Cs/Chs-FA is highly promoted by folate receptor mediated uptake mechanism. These results

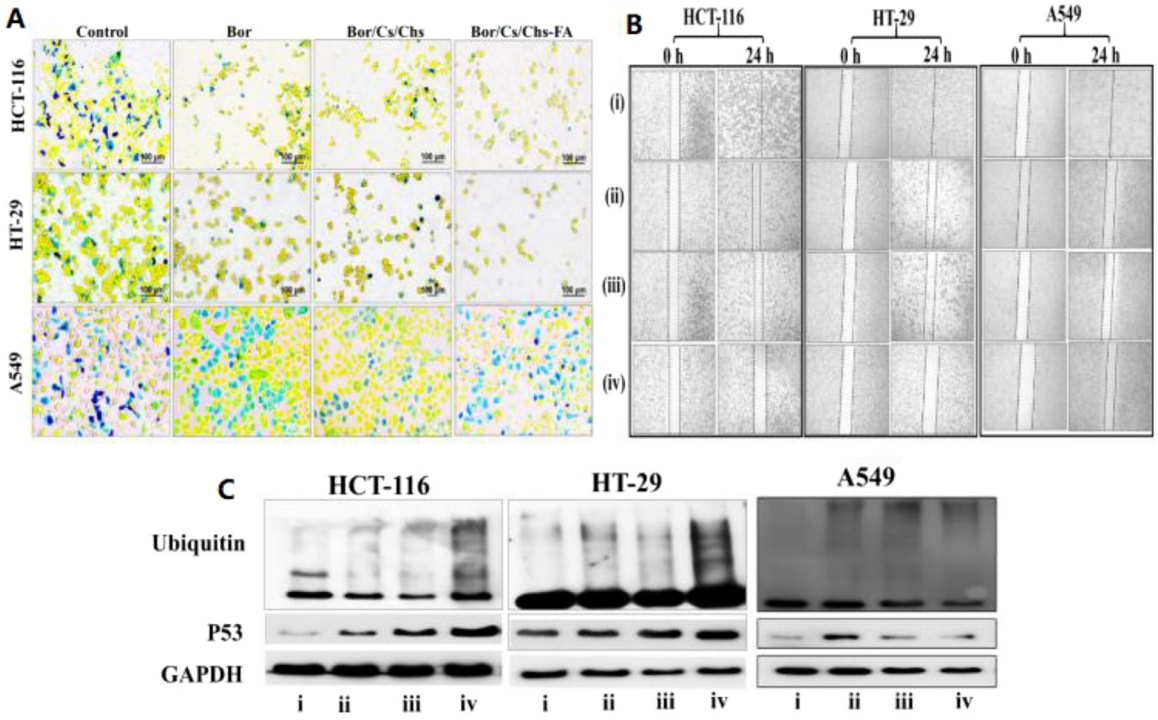

Fig. 5 – (A) Distribution of cells in cell cycle phases, G1, G2, M, and S phase after 24 h treatment with Bor, Bor/Cs/Chs, and Bor/Cs/Chs-FA (Bor/Cs&Chs/FA weight ratios, 1:2:1) in folate receptor positive human colorectal cancer cells, HCT-116 and HT-29, and folate receptor negative lung cancer cell line, A549, was visualized by fluorescence microscopy. Scale bars represent 100 μm. (B) Cell migration efficiency after 24 h treatment with (i) control, (ii) Bor, (iii) Bor/Cs/Chs, and (iv) Bor/Cs/Chs-FA in folate receptor positive human colorectal cancer cells, HCT-116 and HT-29, and folate receptor negative lung cancer cell line, A549. (C) Western blot analysis in stated cells following incubation with (i) control, (ii) Bor, (iii) Bor/Cs/Chs, and (iv) Bor/Cs/Chs-FA (v) by using specific proteins, P53 and Ubiquitin. GAPDH was used as a control.

also highlight the effect of folate targeting ligand in efficacy of formulations.

To observe the effect of Bor/Cs/Chs-FA on the migration ability of colorectal cancer cells, wound healing assay was performed. The results showed that the cell population of HCT-116 and HT-29 treated with Bor/Cs/Chs-FA was significantly lower in the area between the scratched edges than that in the control and free drug conditions (Fig. 5B). However, area between the scratched edges of A549 cells after treatment with Bor/Cs/Chs-FA was similar to that after treatment with non-targeted nanoparticles (Bor/Cs/Chs). This shows that Bor/Cs/Chs-FA was able to inhibit migration and invasion mediated by FA receptor *in vitro*.

Furthermore, the effect of Bor/Cs/Chs-FA on the expression of different apoptotic proteins was investigated in both folate receptor expressing and deficient cell lines by western blot analysis (Fig. 5C, S6). The expressions of apoptotic marker, P53, and Bor specific marker, ubiquitin, in folate receptor expressing colorectal cancer cells treated with Bor/Cs/Chs-FA were significantly enhanced as compared with control, free drug, and Bor/Cs/Chs treatments. However, no such elevation in apoptotic protein levels was observed in folate receptor deficient cell line A549. These data showed that Bor/Cs/Chs-FA could increase the number of cells in late apoptotic phase via folate targeted DSPE-PEG of nanoparticles.

3.4. *In vivo antitumor effects*

HCT-116 tumor bearing xenograft mice model was developed to analyze the *in vivo* antitumor effect of Bor/Cs/Chs-FA on colorectal cancer. Bor/Cs/Chs-FA could inhibit the tumor progression by early DNA fragmentation coupled with apoptosis, which enhanced its antitumor effect on folate receptor overexpressing colorectal cancer (Fig. 6A). This significant improvement in antitumor effect suggested that the relationship between folate targeted nanoparticles and folate receptors on cancer cells could play a vital role in chemotherapy. In addition, after checking tumor volume and body weight in the control and treatment groups, we can conclude that folate targeted delivery of Bor/Cs/Chs to cancer cells with ability of a prolonged systemic circulation resulted in minimization of untoward effects (Fig. 6B). Moreover, tumor cell apoptosis was increased by inhibition of tumor cell proliferation and angiogenesis mechanisms without toxicological signs on the five principal organs at histological level, as shown by H & E staining (Fig. 6C, Table S2). The levels of CD31 and Ki-67, cell proliferation and angiogenesis markers, were significantly decreased in tumor tissues treated with Bor/Cs/Chs-FA than in those treated with free drug, and non-targeted nanoparticles. Furthermore, high level of apoptotic markers, caspase-3 and PARP, which promote cancer cell apoptosis and angiogenesis, and proliferation were observed in cells treated with

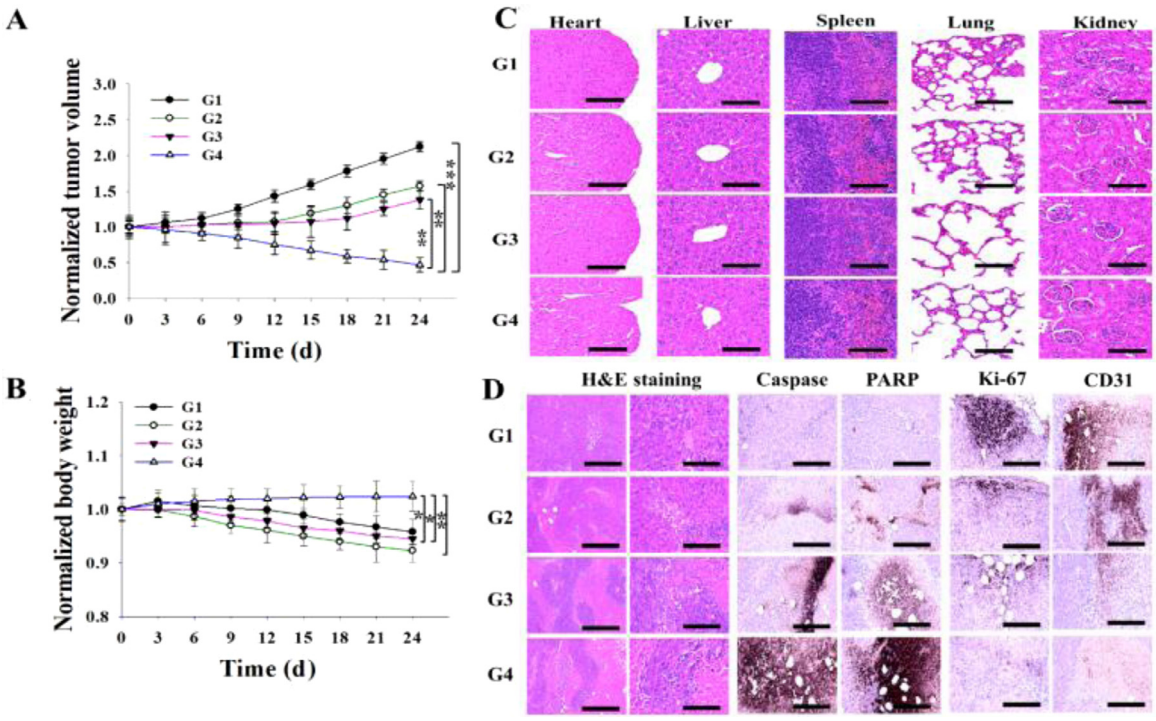

Fig. 6 – *In vivo* antitumor studies on (A) tumor volume, (B) body weight, and (C) histopathological changes of organs (heart, liver, spleen, lungs, and kidneys) following intravenous administration of different formulations (control, Bor, Bor/Cs/Chs, and Bor/Cs/Chs-FA (Bor/Cs&Chs/FA weight ratios, 1:2:1)) to HCT-116 tumor bearing BALB/c nude mice. Each formulation was administered four times at three-day intervals (*P < 0.05, **P < 0.01,). (D) Immuno-histopathological analyses. Representative changes in tumor histopathology and immunoreactivity to caspase-3, PARP, Ki-67, and CD31 in tumor masses of nude mice following treatment with the indicated formulations are shown. Caspase-3 and PARP are markers for apoptosis and CD31 and Ki-67 are markers for angiogenesis. Scale bar is 120 μm.

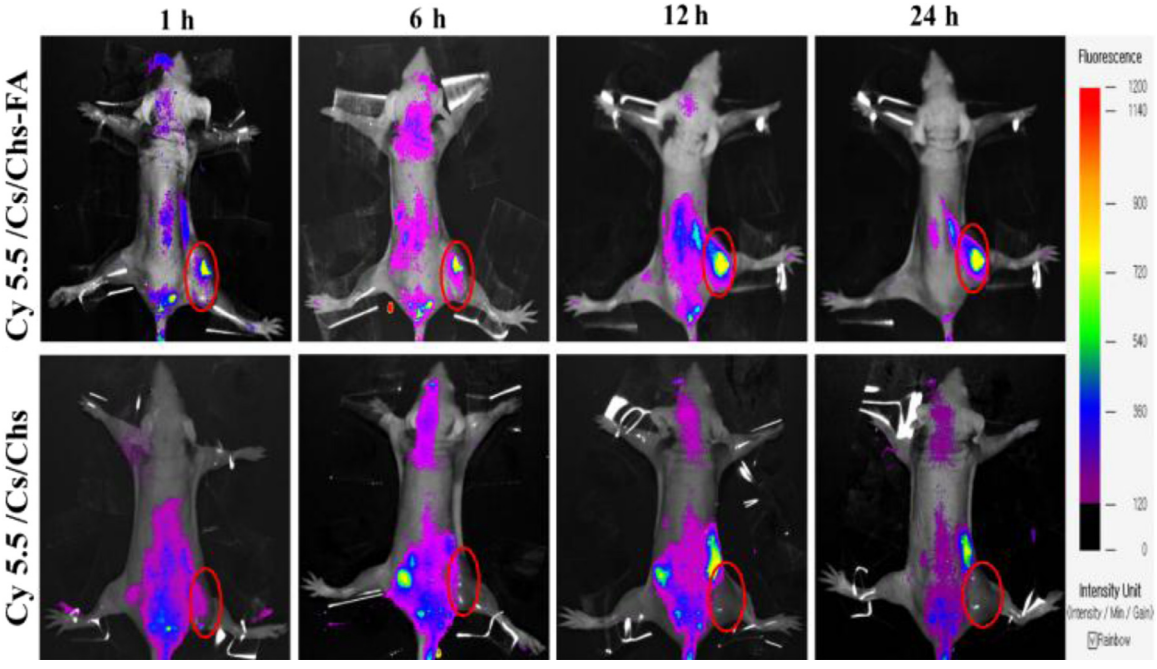

Fig. 7 – *In vivo* biodistribution fluorescence imaging of subcutaneous HCT-116 tumor-bearing BALB/c nude mice after iv injection of 100 μl cyanine 5.5 loaded Bor/Cs/Chs-FA (Bor/ Cs&Chs/FA weight ratios, 1:2:1) and Bor/Cs/Chs (both containing 1 μg/ml cyanine 5.5).

Bor/Cs/Chs-FA (Fig. 6D, Table S3). This *in vivo* antitumor study proved that Bor/Cs/Chs-FA could successfully deliver Bor to cancer cells via folate targeted nanoparticles and exert the antitumor effects by inhibiting tumor cell proliferation and inducing cellular apoptosis by activating immune cells.

3.5. *Biodistribution studies*

In vivo fluorescence imaging was carried out to estimate the distribution ability of targeted nanoparticles in tumor area and other vital organs. Cy 5.5 was used as the fluorescence marker. After injection of Cy 5.5 loaded targeted nanoparticles and Cy 5.5 loaded non-targeted nanoparticles into the tail veins of mice models, fluorescence was immediately distributed throughout the body in both injected groups (Fig. 7). However, the fluorescence intensity in the tumor area of group injected Cy 5.5 loaded targeted nanoparticles was much higher than that of nontargeted nanoparticles, suggesting that the folate targeted nanoparticles could enhance the drug delivery and accumulation of nanoparticles into targeted tumor areas. After 24 h, fluorescence intensity of dissected organs (heart, liver, spleen, lung, and kidney) and tumor tissue were checked. If nanoparticle could distribute *in vivo* for an acceptable time to release the drug in the tumor area, an enhanced permeability and retention (EPR) effect is likely to be obtained with reduction of cardiotoxicity. Thus, we suggest that Bor/Cs/Chs-FA highly accumulates in tumor area and shows low non-specific uptake in reticuloendothelial system (RES). This in turn facilitates uptake of folate targeted nanoparticles to folate receptor overexpressing cancers via the receptor-mediated endocytosis [53].

4. Conclusion

In conclusion, Bor was successfully encapsulated in folate-targeted Cs/Chs complex nanoparticles. Bor/Cs/Chs-FA had high drug loading capacity with nano-sized particles. The efficacy of inducing apoptosis and cellular uptake efficiency of Bor/Cs/Chs-FA in folate receptor overexpressing cancer cells were enhanced by using biocompatible and biodegradable polysaccharides complexed nanocarriers which allow the sustained release and improve loading capacity of Bor. *In vivo* antitumor studies in HCT-116 xenograft mice revealed that Bor/Cs/Chs-FA mediated a greater suppression of xenograft tumors with lesser toxicity to normal organs and tissues as compared to those of control, free drugs, and formulation without folate targeting ligand. Hence, our optimized formulation may be beneficial in folate-receptor-targeted chemotherapy, leading to be potential candidates for treatment of folate receptor overexpressing colorectal cancers.

Declaration of interest

The authors report no conflicts of interest. The authors alone are responsible for the content and writing of this article.

Acknowledgment

This research was supported by the Yeungnam University research grant in 2017.

Supplementary materials

Supplementary material associated with this article can be found, in the online version, at doi:10.1016/j.ajps.2018.09.004.

REFERENCES

[1] Sim T, Lim C, Hoang NH, Oh KT. Recent advance of pH-sensitive nanocarriers targeting solid tumors. J Pharm Investig 2017;47(5):383–94.
[2] De Rosa M, Pace UGO, Rega D, et al. Genetics, diagnosis and management of colorectal cancer (Review). Oncol Rep 2015;34(3):1087–96.
[3] Jabir NR, Tabrez S, Ashraf GM, Shakil S, Damanhouri GA, Kamal MA. Nanotechnology-based approaches in anticancer research. Int J Nanomedicine 2012;7:4391–408.
[4] Mousa SA, Bharali DJ. Nanotechnology-based detection and targeted therapy in cancer: nano-bio paradigms and applications. Cancers (Basel) 2011;3(3):2888–903.
[5] Choi YH, Han HK. Nanomedicines: current status and future perspectives in aspect of drug delivery and pharmacokinetics. J Pharm Investig 2018;48(1):43–60.
[6] Hoang NH, Lim C, Sim T, Oh KT. Triblock copolymers for nano-sized drug delivery systems. J Pharm Investig 2017;47(1):27–35.
[7] Gupta B, Yong CS, Kim JO. Solid matrix-based lipid nanoplatforms as carriers for combinational therapeutics in cancer. J Pharm Investig 2017;47(6):461–73.
[8] Ruttala HB, Ramasamy T, Madeshwaran T, et al. Emerging potential of stimulus-responsive nanosized anticancer drug delivery systems for systemic applications. Arch Pharm Res 2018;41(2):111–29.
[9] Richards DA, Maruani A, Chudasama V. Antibody fragments as nanoparticle targeting ligands: a step in the right direction. Chem Sci 2017;8(1):63–77.
[10] Kim CH, Lee SG, Kang MJ, Lee S, Choi YW. Surface modification of lipid-based nanocarriers for cancer cell-specific drug targeting. J Pharm Investig 2017;47(3):203–27.
[11] Jin E, Zhang B, Sun X, et al. Acid-active cell-penetrating peptides for *in vivo* tumor-targeted drug delivery. J Am Chem Soc 2013;135(2):933–40.
[12] Li P, Wang Y, Zeng F, Chen L, Peng Z, Kong LX. Synthesis and characterization of folate conjugated chitosan and cellular uptake of its nanoparticles in HT-29 cells. Carbohydr Res 2011;346(6):801–6.
[13] Han S, Liu Y, Nie X, et al. Efficient delivery of antitumor drug to the nuclei of tumor cells by amphiphilic biodegradable poly(l-aspartic acid-co-lactic acid)/DPPE co-polymer nanoparticles. SMALL 2012;8(10):1596–606.
[14] Zhu Y, Liao L. Applications of nanoparticles for anticancer drug delivery: a review. J Nanosci Nanotechnol 2015;15(7):4753–73.
[15] Nair R, Reddy BH, Kumar CA, Kumar KJ. Application of chitosan microspheres as drug carriers: a review. J Pharm Sci and Res 2009;1(2):1–12.

[16] Chen Y, Mohanraj VJ, Parkin JE. Chitosan-dextran sulfate nanoparticles for delivery of an anti-angiogenesis peptide. LIPS 2003;10(5–6):621–9.
[17] Luo Y, Wang Q. Recent development of chitosan-based polyelectrolyte complexes with natural polysaccharides for drug delivery. Int J Biol Macromol 2014;64:353–67.
[18] Janes KA, Fresneau MP, Marazuela A, Fabra A, Alonso MJ. Chitosan nanoparticles as delivery systems for doxorubicin. J Control Release 2001;73(2):255–67.
[19] Sui W, Huang L, Wang J, Bo Q. Preparation and properties of chitosan chondroitin sulfate complex microcapsules. Colloids Surf B 2008;65(1):69–73.
[20] Huang L, Sui W, Wang Y. Preparation of chitosan/chondroitin sulfate complex microcapsules and application in controlled release of 5-fluorouracil. Carbohydr Polym 2010;80(1):168–73.
[21] Kaur G, Rana V, Jain S, Tiwary AK. Colon delivery of budesonide: evaluation of chitosan–chondroitin sulfate interpolymer complex. AAPS PharmSciTech 2010;11(1):36–45.
[22] Umerska A, Corrigan OI, Tajber L. Design of chondroitin sulfate-based polyelectrolyte nanoplexes: Formation of nanocarriers with chitosan and a case study of salmon calcitonin. Carbohydr Polymers 2017;156:276–84.
[23] Accardi F, Toscani D, Bolzoni M, Dalla PB, Aversa F, Giuliani N. Mechanism of action of bortezomib and the new proteasome inhibitors on myeloma cells and the bone microenvironment: impact on myeloma-induced alterations of bone remodeling. Biomed Res Int 2015;2015:172458.
[24] Selimovic D, Porzig BBOW, El-Khattouti A, Badura HE, Ahmad M, Ghanjati F, et al. Bortezomib/proteasome inhibitor triggers both apoptosis and autophagy-dependent pathways in melanoma cells. Cellular Signal 2013;25(1):308–18.
[25] Yu HC, Hou DR, Liu CY, et al. Cancerous inhibitor of protein phosphatase 2a mediates bortezomib-induced autophagy in hepatocellular carcinoma independent of proteasome. PLOS ONE 2013;8(2):e55705.
[26] Rodrigues S, Cardoso L, da Costa AMR, Grenha A. Biocompatibility and stability of polysaccharide polyelectrolyte complexes aimed at respiratory delivery. Materials (Basel) 2015;8(9):5647–70.
[27] Soe ZC, Thapa RK, Ou W, et al. Folate receptor-mediated celastrol and irinotecan combination delivery using liposomes for effective chemotherapy. Colloids Surf B 2018;170:718–28.
[28] Ramasamy T, Sundaramoorthy P, Ruttala HB, et al. Polyunsaturated fatty acid-based targeted nanotherapeutics to enhance the therapeutic efficacy of docetaxel. Drug Deliv 2017;24(1):1262–72.
[29] Tran TH, Nguyen HT, Tran TTP, et al. Combined photothermal and photodynamic therapy by hyaluronic acid-decorated polypyrrole nanoparticles. Nanomedicine (Lond) 2017;12(12):1511–23.
[30] Kirtane AR, Narayan P, Liu G, Panyam J. Polymer-surfactant nanoparticles for improving oral bioavailability of doxorubicin. J Pharm Investig 2017;47(1):65–73.
[31] Thapa RK, Nguyen HT, Gautam M, et al. Hydrophobic binding peptide-conjugated hybrid lipid-mesoporous silica nanoparticles for effective chemo-photothermal therapy of pancreatic cancer. Drug Deliv 2017;24(1):1690–702.
[32] Poudel BK, Gupta B, Ramasamy T, et al. Development of polymeric irinotecan nanoparticles using a novel lactone preservation strategy. Int J Pharm 2016;512(1):75–86 .
[33] Thapa RK, Nguyen HT, Jeong JH, et al. Synergistic anticancer activity of combined histone deacetylase and proteasomal inhibitor-loaded zein nanoparticles in metastatic prostate cancers. Nanomedicine: NBM 2017;13(3):885–96.
[34] Ruttala HB, Ramasamy T, Gupta B, Choi H-G, Yong CS, Kim JO. Multiple polysaccharide-drug complex-loaded liposomes: a unique strategy in drug loading and cancer targeting. Carbohydr Polymers 2017;173:57–66.
[35] Ma X, Williams RO. Polymeric nanomedicines for poorly soluble drugs in oral delivery systems: an update. J Pharm Investig 2018;48(1):61–75.
[36] Zhuo X, Lei T, Miao L, et al. Disulfiram-loaded mixed nanoparticles with high drug-loading and plasma stability by reducing the core crystallinity for intravenous delivery. J Colloid Interface Sci 2018;529:34–43.
[37] Han SM, Na YG, Lee HS, et al. Improvement of cellular uptake of hydrophilic molecule, calcein, formulated by liposome. J Pharm Investig 2018;48(5):595–601.
[38] Tran TH, Nguyen AN, Kim JO, Yong CS, Nguyen CN. Enhancing activity of artesunate against breast cancer cells via induced-apoptosis pathway by loading into lipid carriers. Artif Cells Nanomed Biotechnol 2016;44(8):1979–87.
[39] Thapa RK, Nguyen HT, Jeong JH, et al. Progressive slowdown/prevention of cellular senescence by CD9-targeted delivery of rapamycin using lactose-wrapped calcium carbonate nanoparticles. Sci Rep 2017;7:43299.
[40] Tran TH, Nguyen HT, Le NV, et al. Engineering of multifunctional temperature-sensitive liposomes for synergistic photothermal, photodynamic, and chemotherapeutic effects. Int J Pharm 2017;528(1–2):692–704.
[41] Arora S, Tandon S. Mitochondrial pathway mediated apoptosis and cell cycle arrest triggered by aqueous extract of wheatgrass in colon cancer colo-205 cells. J Plant Biochem Biotechnol 2016;25(1):56–63.
[42] Choi JS, Kim JW, Kim KY, Ku SK, Sohn JH. Single-dose oral toxicity of fermented rice extracts (FREs): a 14-day observation. Pak J Pharm Sci 2014;27(1):129–37.
[43] Kim HS, Park SI, Choi SH, et al. Single oral dose toxicity test of blue honeysuckle concentrate in mice. Toxicol Res 2015;31(1):61–8.
[44] Choi JY, Ramasamy T, Tran TH, et al. Systemic delivery of axitinib with nanohybrid liposomal nanoparticles inhibits hypoxic tumor growth. J Mater Chem B 2015;3(3):408–16.
[45] Gupta B, Pathak S, Poudel BK, et al. Folate receptor-targeted hybrid lipid-core nanocapsules for sequential delivery of doxorubicin and tanespimycin. Colloids Surf B 2017;155:83–92.
[46] Zheng M, Zhao P, Luo Z, et al. Robust ICG theranostic nanoparticles for folate targeted cancer imaging and highly effective photothermal therapy. ACS Appl Mater Interfaces 2014;6(9):6709–16.
[47] Dhanka M, Shetty C, Srivastava R. Injectable methotrexate loaded polycaprolactone microspheres: physicochemical characterization, biocompatibility, and hemocompatibility evaluation. Mater Sci Eng C 2017;81:542–50.
[48] Ruttala HB, Ramasamy T, Shin BS, Choi H-G, Yong CS, Kim JO. Layer-by-layer assembly of hierarchical nanoarchitectures to enhance the systemic performance of nanoparticle albumin-bound paclitaxel. Int J Pharm 2017;519(1):11–21.
[49] Jardim KV, Joanitti GA, Azevedo RB, Parize AL. Physico-chemical characterization and cytotoxicity evaluation of curcumin loaded in chitosan/chondroitin sulfate nanoparticles. Mater Sci Eng C 2015;56:294–304.
[50] Patrulea V, Ostafe V, Borchard G, Jordan O. Chitosan as a starting material for wound healing applications. Eur J Pharm Biopharm 2015;97:417–26.
[51] Jin H, Pi J, Yang F, et al. Folate-chitosan nanoparticles loaded with ursolic acid confer anti-breast cancer activities *in vitro* and *in vivo*. Sci Rep 2016;6:30782.
[52] Maya S, Sarmento B, Lakshmanan VK, Menon D, Seabra V, Jayakumar R. Chitosan cross-linked docetaxel loaded EGF receptor targeted nanoparticles for lung cancer cells. Int J Biol Macromol 2014;69:532–41.
[53] Thapa RK, Byeon JH, Ku SK, Yong CS, Kim JO. Easy on-demand self-assembly of lateral nanodimensional hybrid graphene oxide flakes for near-infrared-induced chemothermal therapy. NPG Asia Mater 2017;9:e416.